

MEASUREMENT OF MEMBRANE DISPLACEMENT WITH A MOTIONLESS CAMERA EQUIPPED WITH A FIXED FOCUS LENS

Krzysztof Murawski

Military University of Technology, Institute of Teleinformatics and Automatics, Kaliskiego Str. 2, 00-908 Warsaw, Poland,
(✉k.murawski@ita.wat.edu.pl), IEEE Member #...92707852

Abstract

The paper presents a technique for measuring membrane displacements with one motionless camera. The method consists in measuring the distance to an object based on one image obtained from a motionless camera with a fixed-focus lens. The essence of the proposed measurement technique is to determine changes of the distance between a membrane and a video camera based on analysis of changes in the focus view of a marker placed on the membrane plane. It is proven that the used technique allows to monitor the frequency and amplitude of the membrane vibration. The tests were performed for the oscillation frequency in the range from 0.5 Hz to 6 Hz and deviations from the neutral position in the range of ± 3 mm.

Keywords: measurement based on fuzzy signal, diaphragm displacement, image processing, motion sensor.

© 2015 Polish Academy of Sciences. All rights reserved

1. Introduction

Measuring the membrane displacement, the non-contact measurement in particular, has many applications [1, 2]. However, it still generates a lot of problems, especially in difficult conditions [3]. The parameters of the membrane displacement are determined then by measuring other physical quantities. For this reason attempts are made to use fibre pressure sensors [4, 5], piezofolios [3], the Helmholtz resonator [6, 7], optical [8–12] and capacitive sensors [13, 14]. When the dimensions of the sensor do not impose significant limitations, a fluorescence videogrammetry [15] can be used as well as the method described in [16].

This paper presents a new approach to measuring the displacement parameters of a membrane, Fig. 1. The measurement was implemented with a motionless *IR* camera equipped with a fixed focus lens and using an image processing technique shown in chapter 3. The membrane displacement was determined by observing changes in the size of a marker placed on the membrane surface. The membrane displacement parameters were determined in real-time, based on a single photo for measuring the amplitude, and a sequence of photos when the vibration frequency was measured.

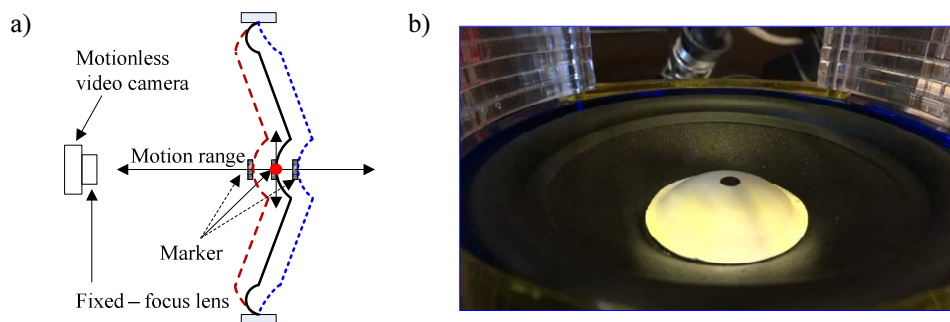


Fig. 1. The displacement model (a), a view of the monitored membrane (b).

The tests were performed in the system presented in Fig. 2. The model in Fig. 2 was equipped with a membrane with a rubber surround, Fig. 1b. The membrane was connected to a voice coil, which was placed in a constant magnetic field. A movement of the membrane was generated by applying DC or AC voltage of a known shape, amplitude and frequency to the connectors of the coil.

2. Measurement system configuration

The frequency and the displacement of the membrane were measured in the measurement system shown in Fig. 2. The main element of the system is the model presented in Fig. 3a.

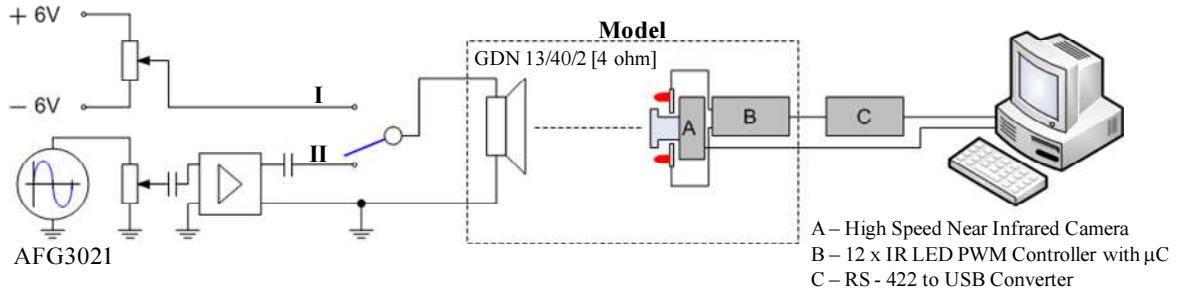


Fig. 2. The system for testing the parameters of the membrane displacement.

The model was developed basing on the membrane of a TONSIL GDN 13/40/02 woofer with the following parameters: the rated frequency range 90 – 5000 Hz, the rated impedance - 4 ohm, the voice coil resistance - 3.45 ohm, the total moving mass - $8.4e^{-3}$ kg, the force factor - 5.03 Tm, the voice coil height - 9 mm, the height of the magnetic gap - 6 mm, the piston area - 85 cm². The model enabled safe moving of the woofer membrane to its rest relative position in the range of ± 3 mm. The membrane is provided with a marker, Fig. 3b, which has been observed in the camera shown in Fig. 3a and Fig. 3c. The camera recorded the view of the marker registered in the near-infrared band ($\lambda=850$ nm) at 60 frame per second (fps). The IR heater construction was discussed in [17, 18]. The developed measuring system has enabled powering the woofer coil with a DC voltage (Fig. 2, switch in position I) and also an AC voltage (Fig. 2, switch in position II). The DC voltage was used to determine the range and direction of the membrane deflection depending on the applied control voltage value, supplying the voice coil.

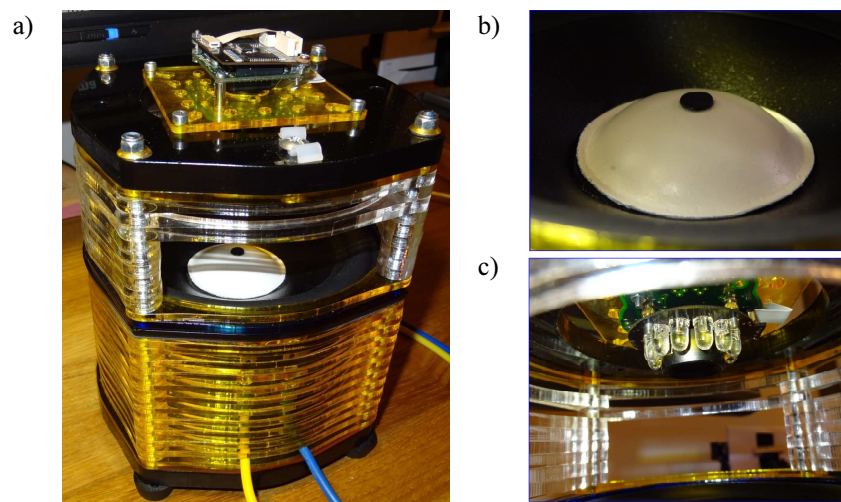


Fig. 3. The construction of the model developed for determining the membrane displacement: the model with a mounted camera (a), a view of the marker (b), a lens and IR heater (c).

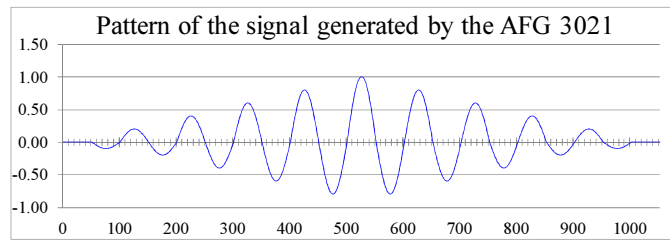


Fig. 4. A sample of the voltage waveform generated by an AFG 3021 generator.

The vibration frequency of the membrane was measured for alternating voltages of a known waveform, amplitude and fixed frequency. The alternating voltage was generated by an AFG 3021 generator. The generator was connected to the woofer through a VM 100 amplifier. The tests were carried out, forcing the membrane displacement by applying an alternating sinusoidal signal with the amplitude close to 12 V and the f_{SET} frequencies 0.5, 0.7, 0.9, 1.0, 1.1, 1.3, 1.5, 2.0, 2.5, 3.0, 3.5, 4.0, 5.0 and 6.0 Hz. The tests for signal pulses with a waveform presented in Fig. 4 were performed for the given system configuration. The generated signal frequencies were: 0.5, 0.7, 0.9, 1.0, 1.1, 1.3, 1.5, 2.0, and 2.5 Hz. The aim of this study was to examine a possibility of determining the membrane displacement parameters in dependence on changes of the control signal amplitude.

3. Image processing technique

The discussed measurement method determines the marker width basing on a single photo. The essence of the presented solution consists in the image analysis [19 – 22] resulting from the object moving away from the position for which the focus was set, Fig. 5.

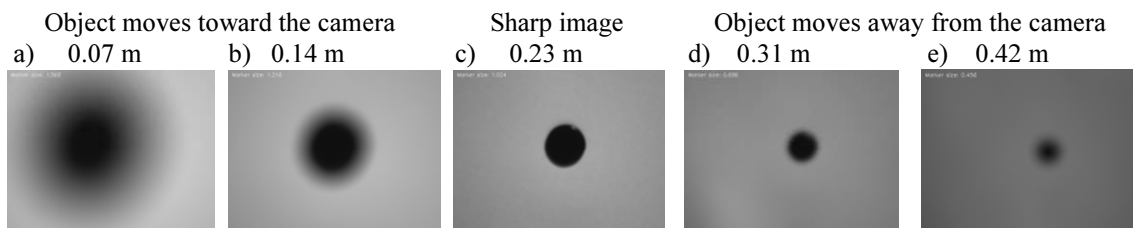


Fig. 5. An exemplary sequence of recorded images.

Figure 6 shows the horizontal line profiles of the images (Fig. 5a, 5c, 5e) indicated by the marker centre of gravity as well as their behaviour during changes of the image focus.

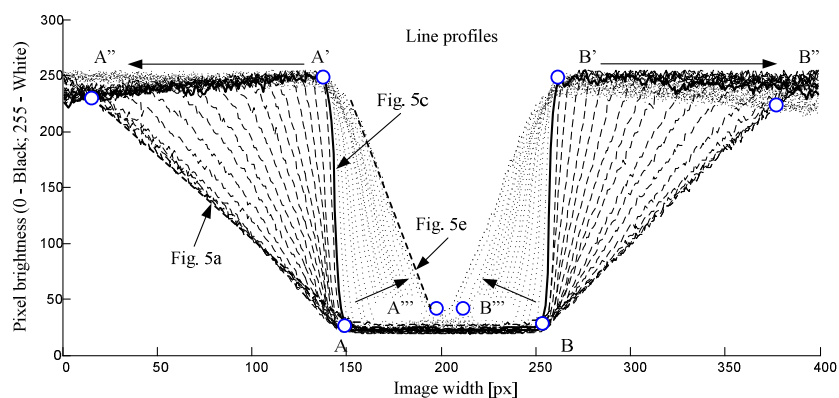


Fig. 6. Horizontal line profiles for the images from Fig. 5a, 5c, 5e determined by the centre of gravity of the object after standardising its brightness.

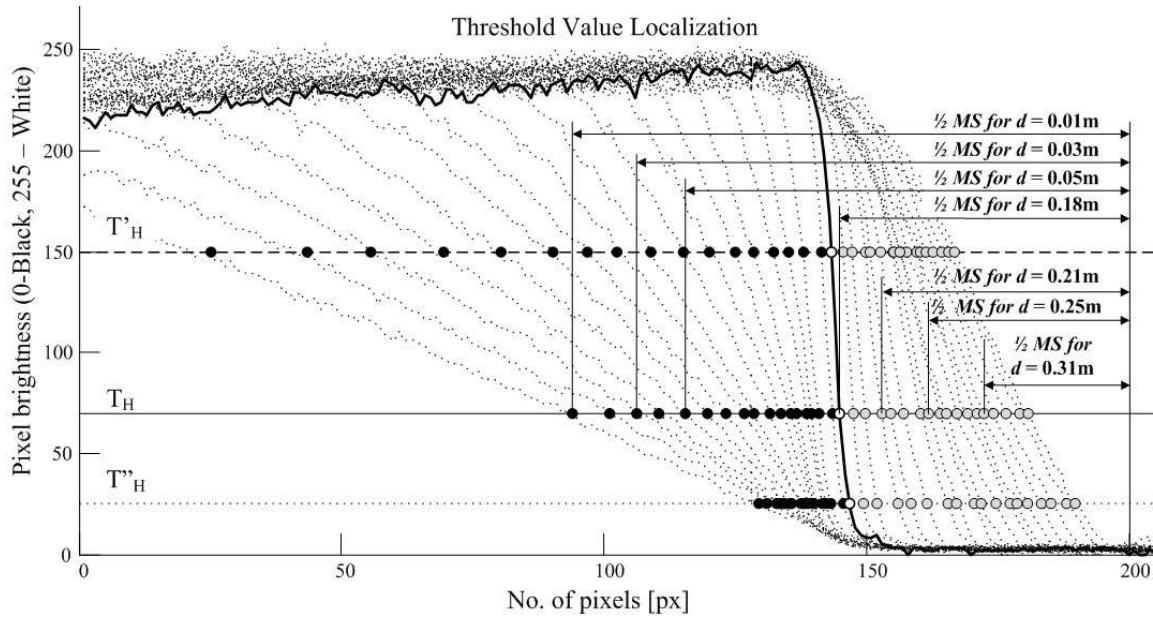


Fig. 7. The distribution of essential points due to determining the distance to the object for the accepted threshold value T_H at $L_{MIN} = 0.07$ m, $L_{MAX} = 0.42$ m and $\Delta L = 0.01$ m.

For the sharp view of the marker, Fig. 5c, sections AA' and BB' in Fig. 6 are almost vertical, which indicates a sharp cut-off of the view of the marker from the background. When the marker gets closer to the camera, its image becomes blurred, Fig. 5a and Fig. 5b. As a result, points A' and B' move, respectively, in the direction of A'' and B''. At the same time, the distance between points A and B remains almost unchanged. When the object with the marker moves away from the camera, points A'' and B'' return back to their initial positions ($A'' \rightarrow A'$, $B'' \rightarrow B'$), and the marker image comes into focus again. Further distancing the marker from the camera results in its image gradually blurring and becoming smaller, Fig. 5d and Fig. 5e. In the considered case, the movement of points $A \rightarrow A'''$ and $B \rightarrow B'''$ is observed. The positions of points A' and B' remain unchanged.

An exemplary sequence of changes in the positions of points A, A', B, B' determined during the marker moving close and moving away from the camera is presented in Fig. 6 and Fig. 7. Changed positions of points A, A', B, B' were used to determine the marker width. For this purpose, the image from the camera was de-blurred. Image de-blurring was performed using the image binarisation with a threshold T_H equal to 70. Selecting the binarisation threshold consists in determining a T_H value assuring a uniform distribution of points intersecting profile image horizontal lines (indicated by the centre of gravity of the marker) with the line illustrating the tested T_H value, Fig. 7. The location of the determined points is unambiguously associated with the marker width MS and its distance d from the camera. The distribution of points is described by the equation (1) in the modelling process. The result is a relation that describes the object distance from the camera as a function of changes in the marker size. The presented modelling process is performed only once.

4. Description of experiments and results of research

4.1. Measuring the membrane vibration frequency

The study was carried out in the set-up shown in Fig. 2, in which the source switch of the signal was set to position II. The sinusoidal wave U_{IN} was applied at the input of the amplifier with the frequency f_{SET} . The waveform amplitude was selected so that the voltage at the output of the amplifier was within the range of ± 5.8 V.

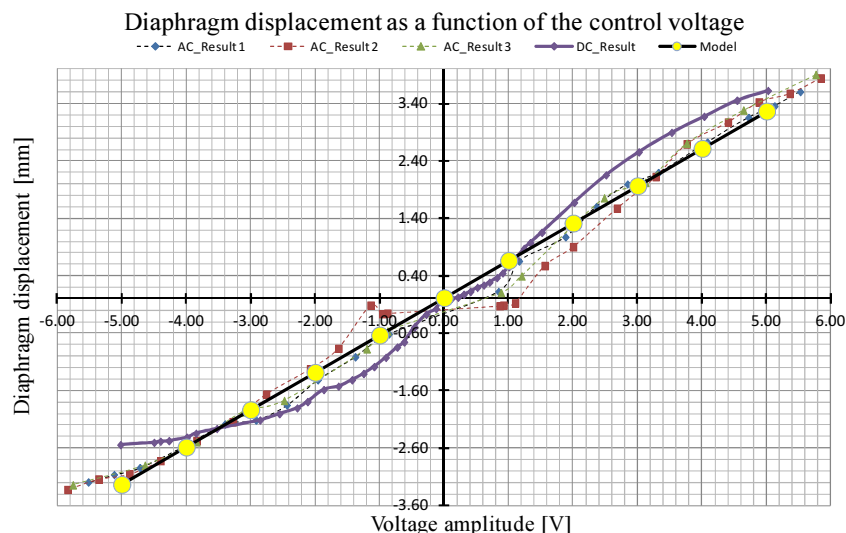


Fig. 8. The diaphragm (membrane) displacement as a function of the control voltage amplitude.

The membrane moved in the range from -3.4 mm to +3.8 mm relative to the position established by the lower and upper resor of the speaker in absence of the voltage control. The dependence of the position of the membrane in the function of the voltage control value is presented in Fig. 8. In the study no significant changes of the membrane position resulting from the occurrence of the hysteresis phenomenon were observed. An influence of the alternating voltage amplitude on the membrane deflection was measured three times. The multiple measurements were repeated to reduce the impact of random errors resulting from the use of a highly sensitive (of 0.01 mm accuracy) dial gauge. The signal resulting from the membrane vibration was obtained using a motionless *IR* camera equipped with a fixed focus lens. The membrane vibration was determined by observing the changes in the size of the marker placed on the membrane surface. A black circular marker of 7 mm diameter was used in the study, Fig. 3b.

Measuring the membrane vibration frequency involved a signal analysis. The signal shape reflects changes in the marker image size in the function of time. These changes were expressed relative to the size of the marker recorded in the rest position. The results obtained for the f_{SET} signal frequencies from 0.5 Hz to 2.5 Hz are presented in Fig. 9.

Determined relative changes in the size of the marker image reflect the nature of the periodic signal which forces a movement of the membrane. The recovered signal, such as the excitation signal, has a periodic nature, and the amplitude change takes on repetitive values within each of the tested frequency bands. A slight change in the size of the marker image, depending on the membrane deflection – Fig. 9, is a result of amplifier parameters used, including its bandwidth.

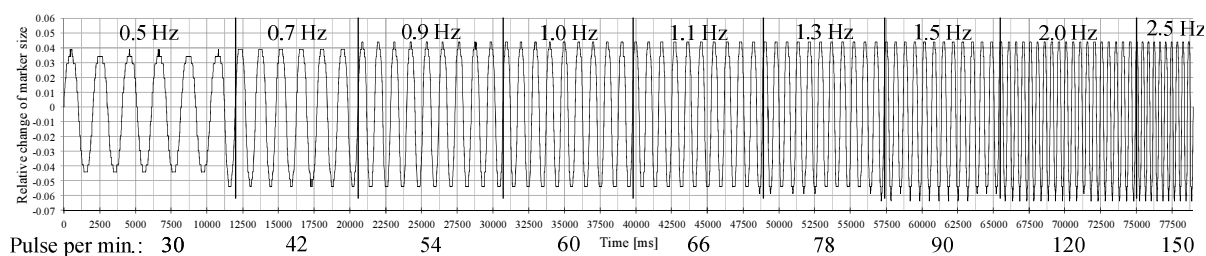


Fig. 9. Changes in the marker image size recorded for the given frequencies.

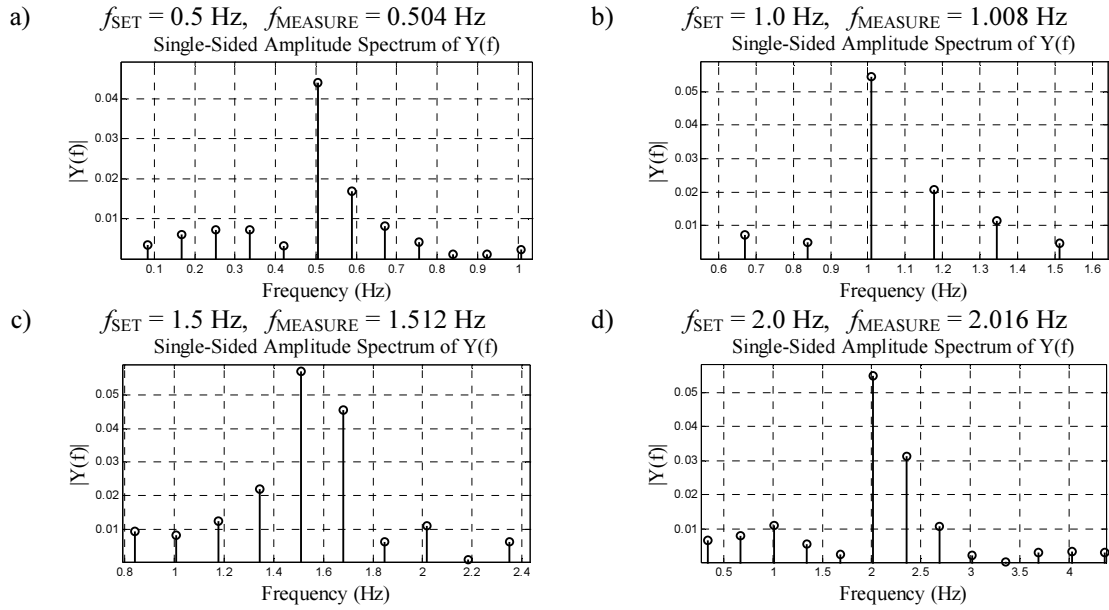


Fig. 10. Examples of signals of amplitude spectrums:
 f_{SET} – the inflicted vibration frequency, f_{MEASURE} – the measured vibration frequency.

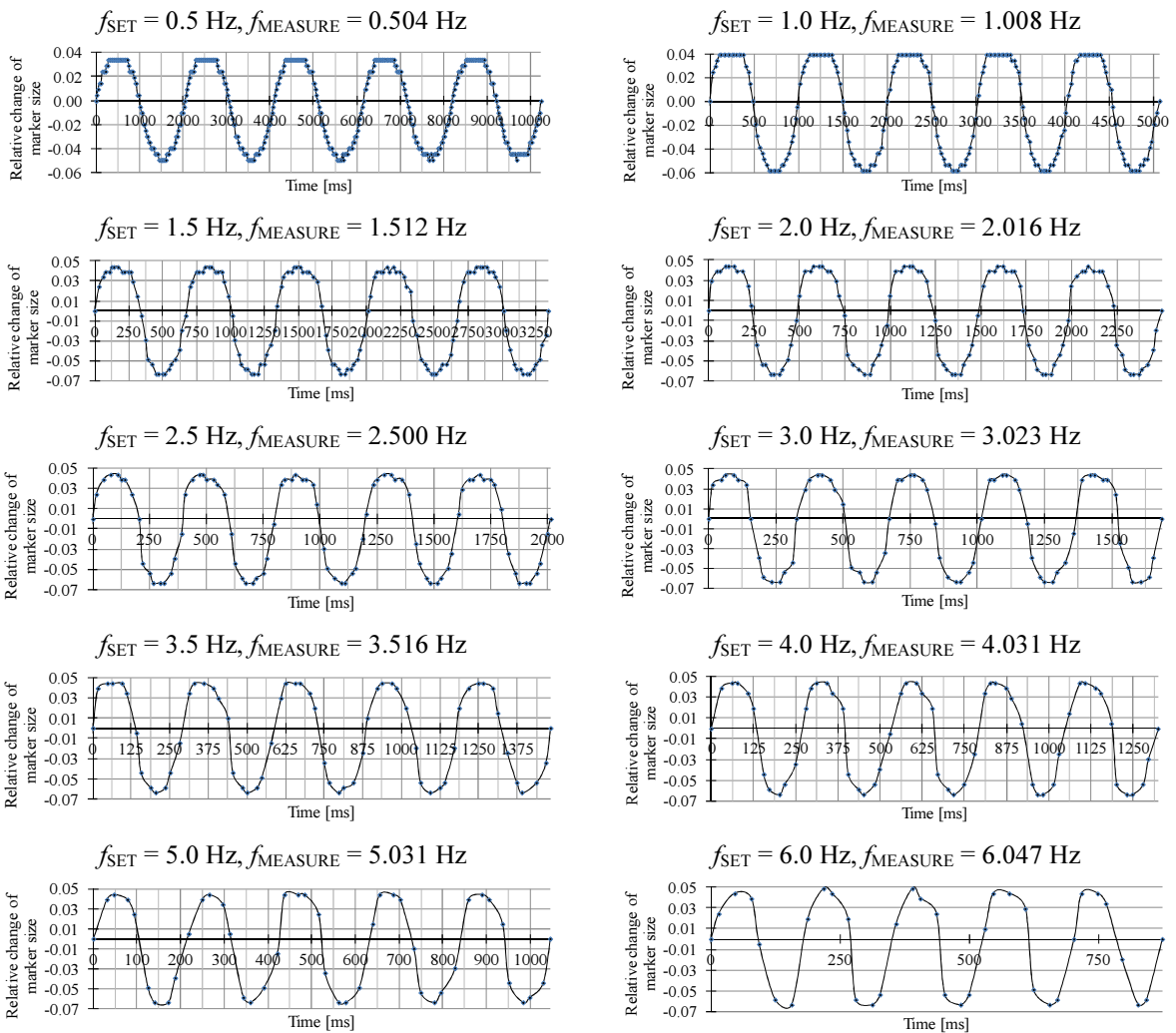


Fig. 11. Results based on the recorded data:
 f_{SET} – the inflicted vibration frequency, f_{MEASURE} – the measured vibration frequency.

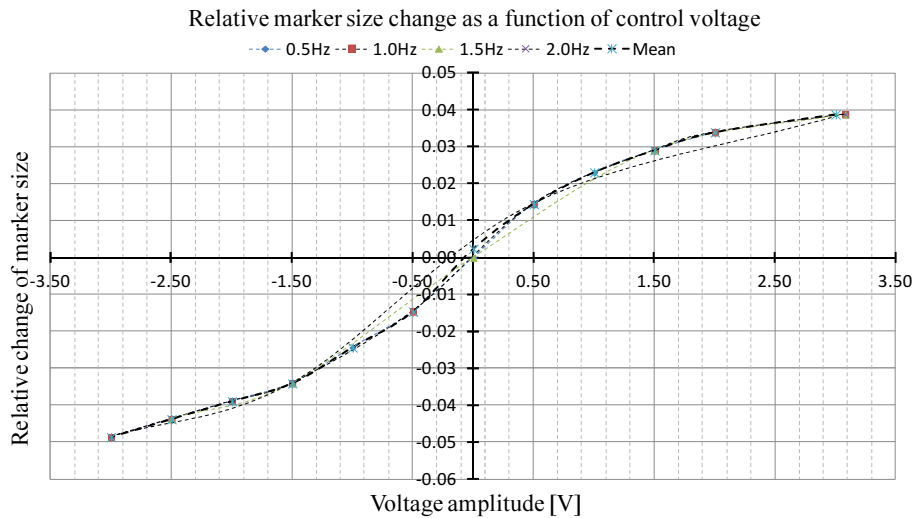


Fig. 12. Changing the size of the marker image observed in the function of changes of the control voltage amplitude.

The vibration frequency of the membrane was determined using Fast Fourier Transform (*FFT*). The sequences of changes in marker image size stored for each input signal were analysed, Fig. 10. For each of them the amplitude spectrum of the *FFT* signal has been computed. Next, the frequency component with a maximum value was searched. This frequency component determines the dominant frequency present in the analysed signal, Fig. 10. The results based on recorded data along with the established f_{SET} and the determined $f_{MEASURE}$ of membrane vibration frequencies are presented in Fig. 11. The length of the sequence in the study was chosen, so that the frequency measurement error using the *FFT* technique was less than 1%. The average percentage error of measuring the membrane vibration frequency was 0.654%.

4.2. Measuring the membrane displacement

The measurement of the membrane displacement was preceded by the calibration procedure, which is performed only once. The purpose of the calibration is to determine the dependence of the membrane displacement y expressed in millimeters on the width of the marker image x . The calibration procedure is carried out in two stages. The first stage is to determine the membrane deflection in a function of the control voltage. The dependence of the membrane deviation on the amplitude of the DC and AC voltage control is presented in Fig. 8. A regression line was determined in the form of function $y(x)=ax + b$ for the carried out measurements. The regression line expresses the dependence of the membrane deflection on the control signal value. The second calibration stage is to record changes in the relative size of the marker for the established voltage values. The study was conducted for alternating voltages with fixed U_{PP} and frequencies of 0.5, 1.0, 1.5 Hz and 2.0 Hz. Changes in the relative size of the marker as well as their averaged values are presented in Fig. 12. The characteristics shown in Fig. 12 are described by the model $M(V, \mu, \sigma, x_m)$ in the form of:

$$M(V, \mu, \sigma, x_m) = v_8 * z^8 + v_7 * z^7 + v_6 * z^6 + v_5 * z^5 + v_4 * z^4 + v_3 * z^3 + v_2 * z^2 + v_1 * z^1 + v_0, \quad (1)$$

for which: the average value of measurements $\mu = 0.0056$; the standard deviation of the measured values $\sigma = 0.0324$; x_m – the measured relative change in the marker size; $z = (x_m - \mu)/\sigma$, $V = \langle v_8, v_7, v_6, v_5, v_4, v_3, v_2, v_1, v_0 \rangle$. The determined parameter values of the model equalled: $v_8 = 0.5029$, $v_7 = 0.1144$, $v_6 = -1.6108$, $v_5 = -0.2557$, $v_4 = 1.6544$,

$v_3 = 0.7893$, $v_2 = -0.6164$, $v_1 = 0.9553$, $v_0 = -0.1861$. The parameters of the model $M(V, \mu, \sigma, x_m)$ can be determined using interpolation algorithms or methods of artificial intelligence [23]. Model $M(V, \mu, \sigma, x_m)$ was used jointly with a simple regression $y(x) = 0.6504x + 0.0102$ (Fig. 8). As a result, the dependency occurring between the measured relative marker size and the membrane displacement expressed in millimetres is presented in Fig. 13.

This dependency is described by the model $M_1(V, \mu, \sigma, x_m)$ of a form (1), for which $\mu = -0.0055$; $\sigma = 0.025547$; $v_8 = 0.046881$, $v_7 = 0.015934$, $v_6 = -0.24341$, $v_5 = -0.058505$, $v_4 = 0.40572$, $v_3 = 0.25788$, $v_2 = -0.24199$, $v_1 = 0.48433$, $v_0 = -0.10785$, where x_m is the measured marker image size. Determining the parameters of the model $M_1(V, \mu, \sigma, x_m)$ concludes the calibration procedure. Measuring the membrane displacement is carried out indirectly by measuring the size of the marker image. The displacement value is calculated from the model $M_1(V, \mu, \sigma, x_m)$ assuming x_m to be the relative marker size obtained during the measurement. By using the model it was possible to determine the value and direction of the membrane displacement, relative to the position of the camera, based on the information obtained from a single image frame. In the setup in Fig. 2 the membrane displacement was determined in less than 16ms. Examples of the results obtained from the analysis of the image sequence are shown in Fig. 14. In the presented case, the amplitude of the voltage controlling the voice coil was within the range of ± 2.5 V. The membrane vibration diagram presented in Fig. 14a was achieved for a sinusoidal input signal with the frequency of 0.5 Hz. The waveform presented in Fig. 14b was created as a result of the voice coil control voltage with the amplitude changed in accordance with the pattern shown in Fig. 4. The frequency parameters of the input signal are presented in Fig. 14b.

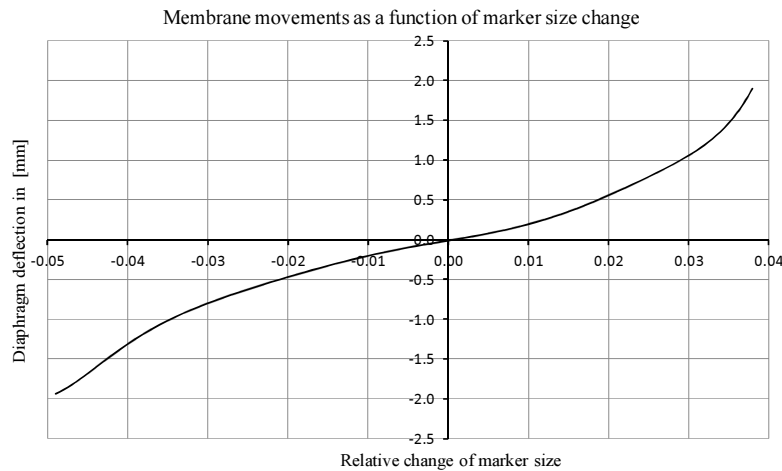
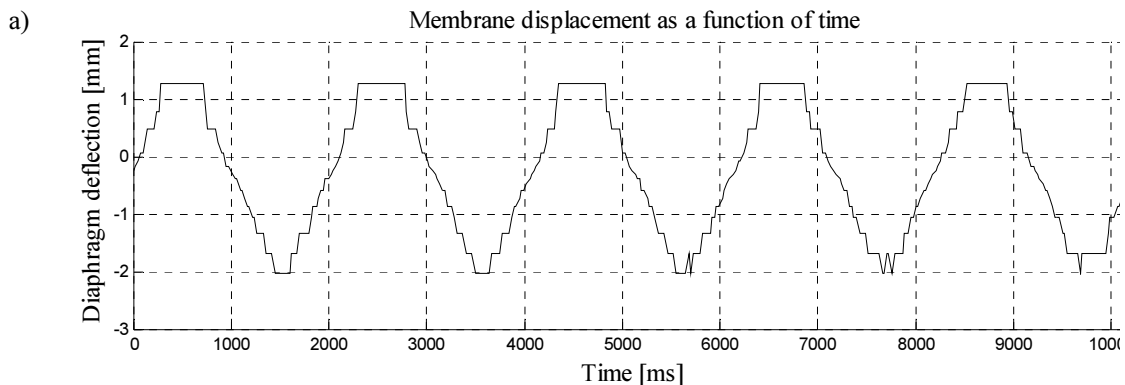


Fig. 13. Changes in the membrane position depending on the determined marker size.



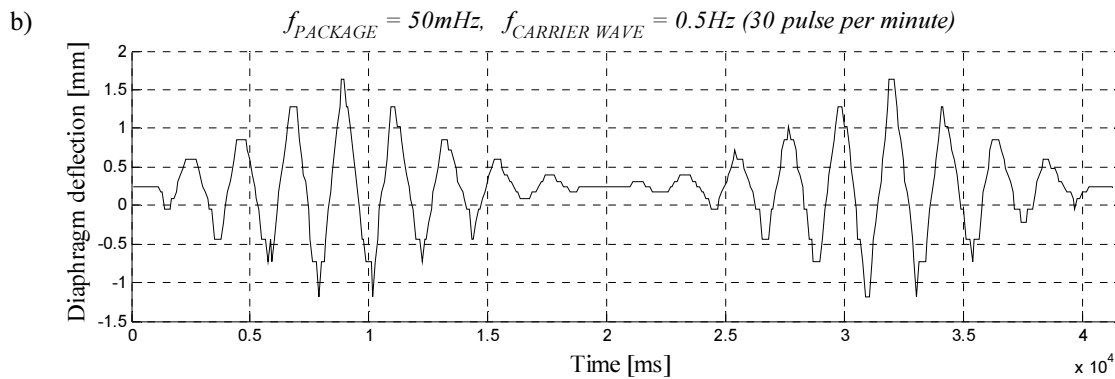


Fig. 14. The membrane displacement determined using the visual technique.

5. Conclusions

The performed experiments have shown that a motionless camera equipped with a fixed focus lens and the image processing technique allow to determine the displacement of a membrane relative to the position of the camera, on the basis of a single image of a marker placed on the membrane. The measurement of the membrane vibration frequency is possible based on the analysis of a series of the marker images.

A camera with a resolution of 640×480 pixels and 60 fps was used in the study. The camera parameters allowed to measure the vibration frequency of the membrane in the range of 0.5 - 6 Hz and the membrane vibration amplitudes in the entire deflection range.

The accuracy of measuring a movement of the membrane in the presented technique is directly proportional to the image resolution. The frequency measurement accuracy increases with the increase in the length of the recorded image sequence. The measured frequency range depends on the number of acquired and analyzed frames per second.

Acknowledgements

The author would like to thank Professor Tadeusz Pustelny as well as Grzegorz Konieczny PhD. Eng. from the Silesian University of Technology, whose publications have been an inspiration for this work.

The work was presented at the 8th Conference Integrated Optics - Sensors, Sensing Structures and Methods, IOS'2014 sponsored by Polish Academy of Sciences. The conference was organized by the Committee of Electronics and Telecommunication at Polish Academy of Sciences in cooperation with the Upper Silesian Division of the Polish Acoustical Society and Photonic Society of Poland, as well as the Department of Optoelectronics at Silesian University of Technology.

References

- [1] VEGA Americas, Inc. (2014). Technologies, Solutions, and Applications - Pressure Measurement.
- [2] WIKA Instrument Corporation. (2014). WIKA Handbook - Pressure & Temperature Measurement U.S. Edition.
- [3] Konieczny, G., Opilski, Z., Pustelny, T., Maciak, E. (2009). State of the work diagram of the artificial heart. *Acta Phys. Pol. A*, 116(3), 344–347.
- [4] Martynkien, T., Szpulak, M., Statkiewicz, G., Golojuch, G., Olszewski, J., Urbanczyk, W., Wojcik, J., Mergo, P., Makara, M., Nasilowski, T., Berghmans, F., Thienpont, H. (2007). Measurements of sensitivity to hydrostatic pressure and temperature in highly birefringent photonic crystal fibers. *Opt. Quant. Electron.*, 39(4-6), 481–489.

- [5] Martynkien, T., Statkiewicz, G., Szpulak, M., Olszewski, J., Golojuch, G., Urbanczyk, W., Wojcik, J., Mergo, P., Makara, M., Nasilowski, T., Berghmans, F., Thienpont, H. (2007). Measurements of polarimetric sensitivity to temperature in birefringent holey fibres. *Meas. Sci. Technol.*, 18(10), 3055–3060.
- [6] Konieczny, G., Opilski, Z., Pustelny, T. (2011). Preliminary research concerning measurements of the POLVAD blood chamber volume based on Helmholtz's acoustic resonator principle. *Acta Phys. Pol. A*, 120(4), 688–692.
- [7] Cirulo, S., Mariscotti, A., Viacava, A. (2009). Helmholtz coil for high frequency high field intensity applications. *Metrol. Meas. Syst.*, XVI (1), 117–127.
- [8] Kisała, P. (2013). Measurement of the maximum value of non-uniform strain using a temperature-insensitive fibre Bragg grating method. *Opto-electronics Review*, 21(3), 293–302.
- [9] Kisała, P. (2012). Application of inverse analysis to determine the strain distribution with optoelectronic method insensitive to temperature changes. *Applied Optics*, 51(16), 3599–3604.
- [10] Detka, M., Kaczmarek, Z. (2013). Distributed strain reconstruction based on a fiber Bragg grating reflection spectrum. *Metrol. Meas. Syst.*, XX (1), 53–64.
- [11] Wierzba, P. (2008). Stability of an optical displacement sensor using a two-beam polarization interferometer. *Metrol. Meas. Syst.*, 15(2), 205–213.
- [12] Dobosz, M. (2012). Laser diode distance measuring interferometer - metrological properties. *Metrol. Meas. Syst.*, XIX (3), 553–564.
- [13] Murugarajan, A., Samuel, G. L. (2011). Measurement, modeling and evaluation of surface parameter using capacitive-sensor-based measurement system. *Metrol. Meas. Syst.*, XVIII (3), 403–418.
- [14] Brecker, H. N., Fromson, R. N., Shum, L. Y. (1977). A capacitance based surface texture measuring system. *Annals of the CIRP*, 25(1), 375–377.
- [15] Dorrington, A. A., Jones, T. W., Danehy, P. M., Pappa, R. S. (2004). Membrane vibration analysis above the Nyquist limit with fluorescence videogrammetry, *Proc. of SEM X International Congress and Exposition on Experimental and Applied Mechanics*, Costa Mesa, CA, United States.
- [16] Binua, S., Mahadevan Pillaia, V. P., Chandrasekaran, N. (2007). Fibre optic displacement sensor for the measurement of amplitude and frequency of vibration. *Optics & Laser Technology*, 39, 1537–1543.
- [17] Różanowski, K., Murawski, K. (2012). An infrared sensor for eye tracking in a harsh car environment. *Acta Phys. Pol. A*, 122(5), 874–879.
- [18] Różanowski, K., Murawski, K. (2013). Optical sensor to monitor pupillary light reflex. *Acta Phys. Pol. A*, 124(3), 558–562.
- [19] Murawski, K. (2010). Method for determining the position of the pupil-based on the labelling algorithm. *Przegląd Elektrotechniczny*, 9, 184–187.
- [20] Murawski, K. (2010). Method for determining the position of the pupil for eyetracking applications. *Proc. XV International Conference on Methods and Models in Automation and Robotics (MMAR)*, 356–362.
- [21] Murawski, K., Różycki, R.; Murawski, P., Matyja, A., Rekas, M. (2013). An infrared sensor for monitoring meibomian gland dysfunction. *Acta Phys. Pol. A*, 124(3), 517–520.
- [22] Murawski, K., Różanowski, K. (2013). Pattern recognition algorithm for eye tracker sensor video data analysis. *Acta Phys. Pol. A*, 124(3), 509–512.
- [23] Murawski, K., Arciszewski, T., De Jong, K. (2000). Evolutionary computation in structural design. *Engineering with Computers*, 16(3-4), 275–286.